# A laser flash photolysis, matrix isolation, and DFT investigation of ($\eta^6$-C$_6$H$_5$Y)Cr(CO)$_3$ (Y = NH$_2$, OCH$_3$, H, CHO, or CO$_2$CH$_3$)

Mohammed A.H. Alamiry [1], Peter Brennan, Conor Long *, Mary T. Pryce

School of Chemical Sciences, Dublin City University, Dublin 9, Ireland

ABSTRACT

The quantum yield for arene displacement from ($\eta^6$-C$_6$H$_5$Y)Cr(CO)$_3$ was measured in 1,1,2-trifluorotrichloroethane (Y = NH$_2$, OCH$_3$, H, CHO, or CO$_2$CH$_3$). Values of 0.24, 0.27, 0.15, 0.17, and 0.32 were obtained respectively ($\lambda_{exc.}$ = 355 nm). These values are significantly higher than those measured for photoinduced arene loss in hydrocarbon solvents using the same excitation wavelength. Laser flash photolysis of ($\eta^6$-C$_6$H$_5$Y)Cr(CO)$_3$ in 1,1,2-trifluorotrichloroethane ($\lambda_{exc.}$ = 355 nm) resulted in the rapid formation (<10 ns) of Cr(CO)$_6$. Matrix isolation experiments on ($\eta^6$-C$_6$H$_5$Y)Cr(CO)$_3$ (Y = H or CHO) at 12 K in CH$_4$ or CO-doped CH$_4$ matrixes using monochromatic irradiation confirmed the presence of two discrete excited states, one leading to CO-loss and the other to arene-loss. The results correlate with the calculated electron drift in the excited state derived from density functional theory and time dependent density functional theory calculations.

© 2008 Elsevier B.V. All rights reserved.

## 1. Introduction

Organometallic compounds often exhibit extensive photochemical properties [1]. For instance the first report which specifically focussed on the photochemistry of simple metal carbonyl compounds appeared in the early 1960s [2]. Subsequent semi-empirical calculations provided an explanation for the relatively high quantum yields for photoinduced decarbonylation in metal carbonyl compounds [3]. Quantum yields ($\Phi$) approach unity in some cases. This coupled with the ease at which the various photo-fragments can be characterised using optical spectroscopy has made metal carbonyl compounds the proto-typical systems in the development of many new photochemical techniques. The rationale for the high quantum yield of CO-loss from Cr(CO)$_6$ ($\Phi_{CO}$ = 0.67 ± 0.01 at 337 nm excitation in cyclohexane) relied on an efficient population of a low-lying Ligand Field (LF) excited state. This state is strongly anti-bonding with respect to the Cr–CO interaction. These studies also suggested that the low-lying Ligand Field (LF) excited state was populated directly upon excitation in a spin allowed but symmetry forbidden transition at the low-energy region of the absorption manifold [4].

Following the development of ab initio methods, in particular Complete Active Space (CASPT2) [5,6] and Density Functional Theory (DFT) [6], the model for the electronic structure of Cr(CO)$_6$ was modified. In particular, the lowest energy transition of Cr(CO)$_6$ is Metal to Ligand Charge Transfer (MLCT) in character and the LF transition, responsible for the CO-loss, is placed at slightly higher energy [7]. The efficiency of the CO-loss process was explained by a coupling of the electronic excited state with vibrational modes, namely the Cr–CO stretching modes, which results in an unbound state with respect to the Cr–CO interaction similar to that proposed by Beach and Gray in their early model [3].

These results have two consequences for the experimental photochemist. Firstly, the vibronic coupling in the excited state breaks the correlation between the absorption process and the subsequent photochemistry. Secondly, the coupling evolves in time, as the wavepacket propagates on the excited state surface. This exposes the photochemical processes to factors that affect this propagation, including vibrational relaxation and the steepness of the multidimensional excited-state surface along specific reaction coordinates [8]. Vibrational relaxation is achieved by coupling with the normal modes and the phonon continuum of the solvent. Consequently the nature of the solvent may have a significant effect on the direction and efficiency of a photochemical process.

In this paper we report the results of our studies on the photochemistry of a series of "half sandwich" compounds of the type ($\eta^6$-C$_6$H$_5$Y)Cr(CO)$_3$ (Y = NH$_2$, OCH$_3$, H, NH$_2$, CHO, or CO$_2$CH$_3$). This system was chosen because it exhibits two photochemical processes, CO-loss and arene-loss. These processes are believed

to result from discrete photo-physical states [9,10]. It is possible to monitor the relative efficiencies of these two processes in different solvents and for various substituents on the arene ring. A range of photochemical techniques were used including, laser flash photolysis, low-temperature matrix isolation, in addition to the standard steady-state methods. The electronic structure and IR spectroscopic properties of the compounds were calculated using DFT methods and the nature of their accessible excited states were obtained from Time Dependent DFT (TDDFT) calculations.

## 2. Results

The IR spectroscopic data for the compounds in this study are presented in Table 1. A comparison of the UV/Vis spectra of $(\eta^6\text{-}C_6H_6)Cr(CO)_3$ and $(\eta^6\text{-}C_6H_5CHO)Cr(CO)_3$ is presented in Fig. 1 showing a $\lambda_{max.}$ at 420 nm for the benzaldehyde compound which is absent in the spectrum of the corresponding benzene compound.

### 2.1. Quantum yield measurements

The quantum yield for the loss of the arene ligand from $(\eta^6\text{-}C_6H_5Y)Cr(CO)_3$ (Y = H, $NH_2$, $OCH_3$, $CO_2CH_3$ or CHO) was measured in CO-saturated cyclohexane or 1,1,2-trifluorotrichloroethane solution using an excitation wavelength ($\lambda_{exc.}$) of 355 nm. All solutions were initially degassed by three cycles of a freeze-pump-thaw method followed by admission of one atmosphere of CO over the solution. The presence of CO has the effect of suppressing the CO-loss process by increasing the efficiency of the reverse reaction with CO and thereby revealing the arene loss process as a reduction in the absorption of the parent compound. As neither $Cr(CO)_6$ nor the free arene compounds absorb significantly at the $\lambda_{max.}$ of the compounds in this study, the reduction in the compound absorbance at its $\lambda_{max.}$ is a measure of the photochemical destruction of the complex (Reactions 1 and 2). The photon flux was measured using standard ferrioxalate actinometry (see Section 5). The results

are presented in Table 2. The quantum yield of arene loss is considerably higher in the halocarbon solvent compared to the hydrocarbon solvent. In addition the quantum yield of arene loss in the halocarbon solvent is significantly higher for Y = $CO_2CH_3$, $NH_2$, and $OCH_3$ than for Y = H or CHO.

### 2.2. UV/Vis flash photolysis of $(\eta^6\text{-}C_6H_5Y)Cr(CO)_3$ in CO-saturated 1,1,2-trifluorotrichloroethane solution at room temperature (Y = $NH_2$, $OCH_3$, or CHO)

A series of ns laser flash photolysis experiments were undertaken to examine the nature of the photochemical events in 1,1,2-trifluorotrichloroethane solution at room temperature. Previous work on these systems in a hydrocarbon solvent (S = cyclohexane) confirmed that the CO-loss product $(\eta^6\text{-}C_6H_5Y)Cr(CO)_2(S)$ was formed with a high quantum yield ($0.72 \pm 15\%$; Y = H) [11]. The $(\eta^6\text{-}C_6H_5Y)Cr(CO)_2(S)$ complex absorbs strongly around 280 nm (Reaction 1) [10]. The time resolved behaviour of this signal was then used to measure the rate constants and activation parameters for the reaction of this solvent stabilised 16 electron species towards CO.

The time resolved behaviour following pulsed photolysis of $(\eta^6\text{-}C_6H_5Y)Cr(CO)_3$ in CO-saturated halo-solvents is different however. For example, a stepwise and persistent change in absorbance was observed following flash photolysis of $(\eta^6\text{-}C_6H_5NH_2)Cr(CO)_3$ at 355 nm in this solvent. When monitored at 330 nm, depletion was observed within the time resolution of the instrument (Fig. 2b), while at 280 nm, an increase in absorption resulted (Fig. 2a). The depletion is the result of the destruction of the parent compound $((\eta^6\text{-}C_6H_5Y)Cr(CO)_3)$ while the increase in absorption can be explained by the rapid formation of $Cr(CO)_6$, which absorbs at 280 nm (Reaction 2). No evidence could be obtained for the presence of precursors to $Cr(CO)_6$ on this timescale. Thus it would appear that changing the solvent from a hydrocarbon to a halocarbon radically alters the nature of the photochemistry both in terms of the products formed and the rate at which they are formed.

**Table 1**
The IR spectroscopic data for the compounds in this study

| Compound | $\nu_{N-N}$ | $\nu_{MC-O}$ | $\nu_{C-O}$ | Medium |
|---|---|---|---|---|
| $(\eta6\text{-}C_6H_6)Cr(CO)_3$ | – | 1978, 1906 | – | 5% CO in $CH_4$ |
| $(\eta^6\text{-}C_6H_5CHO)Cr(CO)_3$ | – | 1995, 1940, 1927 | 1704 | $CH_4$ |
| $(\eta^6\text{-}C_6H_5CHO)Cr(CO)_2$ | – | 1948, 1896 | 1680 | $CH_4$ |
| $(\eta^6\text{-}C_6H_5CO_2CH_3)Cr(CO)_3$ | – | 1991, 1923 | 1735 | $CH_4$ |
| $(\eta^6\text{-}C_6H_5CO_2CH_3)Cr(CO)_2$ | – | 1943, 1890 | – | $CH_4$ |
| $(\eta^6\text{-}C_6H_5CO_2CH_3)Cr(CO)_2N_2$ | 2165 | 1955, 1912 | – | $N_2$ |
| $(\eta^6\text{-}C_6H_5NH_2)Cr(CO)_3$ | – | 1967, 1888 | – | 5% CO in $CH_4$ |
| $(\eta^6\text{-}C_6H_5OCH_3)Cr(CO)_3$ | – | 1976, 1904 | – | $CH_4$ |

**Table 2**
The quantum yields for the decay of $(\eta^6\text{-}C_6H_5Y)Cr(CO)_3$ ($\lambda_{exc.}$ = 355 nm, 20 °C) to form $Cr(CO)_6$ and uncoordinated arene in [a]cyclohexane and [b]1,1,2-trifluortrichloroethane solution

| Y | $\Phi^a$ (±20%) | $\Phi^b$ (±5%) |
|---|---|---|
| $NH_2$ | 0.08 | 0.24 |
| $OCH_3$ | 0.0002 | 0.27 |
| H | 0 | 0.15 |
| CHO | 0.05 | 0.17 |
| $CO_2CH_3$ | 0.0004 | 0.32 |
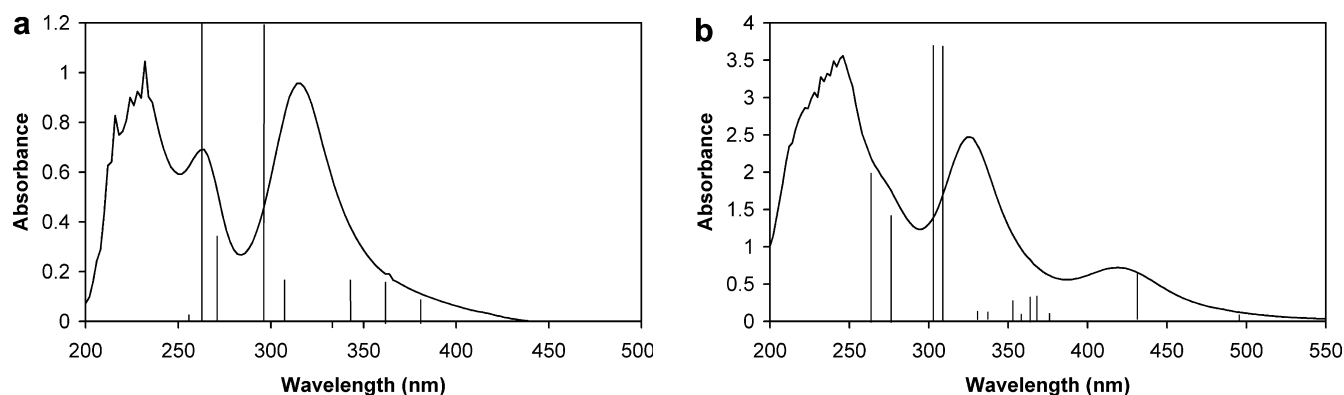


**Fig. 1.** The UV/Vis spectra of $(\eta^6\text{-}C_6H_5Y)Cr(CO)_3$ ((a) Y = H; (b) Y = CHO) in cyclohexane solution at room temperature. The vertical lines represent the calculated transitions obtained from TDDFT calculations (see text for details).
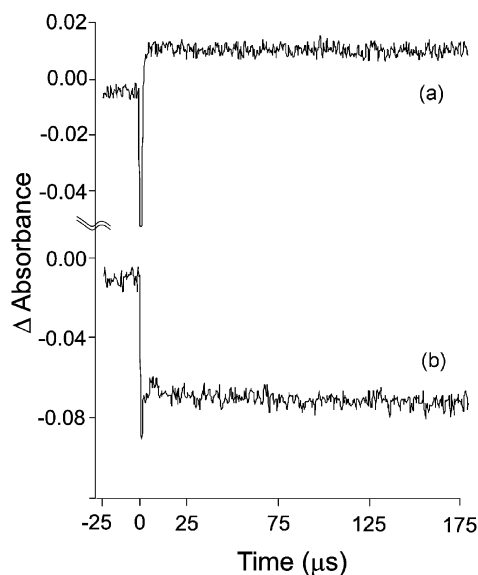
**Fig. 2.** The stepwise change in absorbance observed following pulsed photolysis ($\lambda_{exc.}$ = 355 nm) of ($\eta^6$-$C_6H_5NH_2$)$Cr(CO)_3$ in 1,1,2-trifluorotrichloroethane at room temperature (a) monitored at 280 nm, and (b) monitored at 330 nm.

Reaction 1



Reaction 2
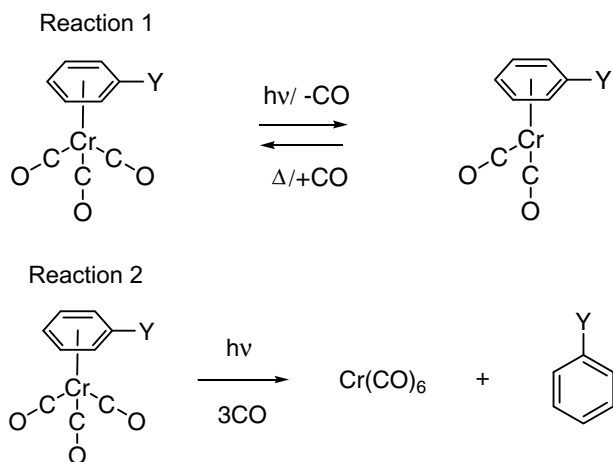


### 2.3. DFT and TDDFT calculations on (($\eta^6$-$C_6H_5Y$)$Cr(CO)_3$ (Y = H, NH_2, OCH_3, CHO or CO_2CH_3)

The theoretical calculations for (($\eta^6$-$C_6H_5Y$)$Cr(CO)_3$ (Y = H, NH_2, OCH_3, CHO or CO_2CH_3) were undertaken to derive a model for the ground state electronic structure of these compounds. The B3LYP hybrid functional was used, as implemented in the GAUSSIAN98 [12], or GAUSSIAN03 [13] programme packages coupled with the double-ξ LanL2DZ basis set. Visualisation of the results was achieved using by GAUSSVIEW [14] and the contribution of orbitals of Cr, CO, and arene ligand were calculated using locally created GAUSSUM [15] software. This model chemistry is a reasonable compromise between accuracy and computational cost and has been shown to produce relatively good results for first row transition metal complexes [16].

All calculations involved the optimisation, without constraints, of the molecular geometry from a starting model obtained from molecular mechanics calculations, followed by calculation of the Hessian matrix to ensure that the system was at a minimum on the potential energy surface. The resulting wavefunction was then subjected to a stability check to confirm the absence of wavefunctions close in energy to the chosen ground state wavefunction. Good agreement between calculated and observed IR frequencies was obtained. The accuracy of the electronic structures was estimated by comparison of the calculated structural and spectroscopic parameters with the experimental values (Tables 3 and 4). More details of these calculations are presented in the Supporting Information.

The optimised geometries were used in the subsequent Time-Dependent DFT (TD-DFT) calculations. The first 20 low-lying excited states of the closed-shell complexes were examined. These calculations provide reasonable estimates of the excitation energies and the oscillator strengths of transitions in these large systems [17–19]. The main focus of these calculations was to determine the nature of the excited states accessible under visible or near UV irradiation. The predicted wavelengths of these transitions are compared with the observed UV/Vis spectrum for ($\eta^6$-$C_6H_6$)$Cr(CO)_3$ and ($\eta^6$-$C_6H_5CHO$)$Cr(CO)_3$ in Fig. 1. The composition

**Table 3**
Table of selected bond lengths calculated and observed (where available) for ($\eta^6$-$C_6H_5Y$)$Cr(CO)_3$ (Y = H, NH_2, OCH_3, CO_2CH_3 or CHO)

| Y | Selected bond | Calculated bond length (Å) | Average measured bond length (Å) |
|---|---|---|---|
| H | Cr–CO[a] | 1.832 | 1.842[b] |
| | CrC–O[a] | 1.188 | 1.158[b] |
| | Cr–C(arene)[a] | 2.317 | 2.229[b] |
| NH_2 | Cr–CO[a] | 1.827 | 1.826[c] |
| | CrC–O[a] | 1.190 | 1.159[c] |
| | Cr–C (arene)[a] | 2.330 | 2.188[c] |
| | C–Y | 1.377 | 1.369[c] |
| OCH_3 | Cr–CO[a] | 1.829 | 1.827[c] |
| | CrC–O[a] | 1.188 | 1.149[c] |
| | Cr–C (arene)[a] | 2.332 | 2.236[c] |
| | C–Y | 1.376 | 1.357[c] |
| CHO | Cr–CO[a] | 1.839 | Not available |
| | CrC–O[a] | 1.185 | Not available |
| | Cr–C (arene)[a] | 2.306 | Not available |
| | C–Y | 1.481 | Not available |
| CO_2CH_3 | Cr–CO[a] | 1.836 | 1.842[d] |
| | CrC–O[a] | 1.185 | 1.154[d] |
| | Cr–C (arene)[a] | 2.308 | 2.220[d] |
| | C–Y | 1.486 | 1.493[d] |

A full listing for each compound is available in the supplementary materials.
[a] Average value presented.
[b] Ref. [39].
[c] Ref. [40].
[d] Ref. [41].

**Table 4**
Selected calculated energy levels (eV) for ($\eta^6$-$C_6H_5Y$)$Cr(CO)_3$ complexes

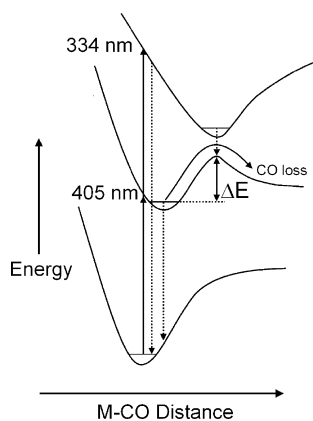| MO | Y | | | | |
|---|---|---|---|---|---|
| | H | NH_2 | OCH_3 | CHO | CO_2CH_3 |
| L+7 | 0.29 | 0.41 | 0.32 | −0.23 | −0.02 |
| L+6 | 0.15 | 0.34 | 0.25 | −0.27 | −0.04 |
| L+5 | 0.15 | 0.17 | 0.20 | −0.63 | −0.18 |
| L+4 | −0.52 | −0.22 | −0.37 | −0.96 | −0.71 |
| L+3 | −0.83 | −0.58 | −0.74 | −1.18 | −0.98 |
| L+2 | −0.83 | −0.70 | −0.84 | −1.20 | −1.00 |
| L+1 | −1.60 | −1.03 | −1.26 | −1.87 | −1.66 |
| LU | −1.60 | −1.41 | −1.55 | −2.89 | −2.48 |
| HO | −6.02 | −5.70 | −5.89 | −6.43 | −6.22 |
| H−1 | −6.02 | −5.78 | −5.94 | −6.45 | −6.23 |
| H−2 | −6.33 | −6.01 | −6.20 | −6.71 | −6.51 |
| H−3 | −9.08 | −7.23 | −7.84 | −7.81 | −8.24 |
| H−4 | −9.08 | −8.89 | −9.06 | −9.21 | −8.76 |
| H−5 | −10.77 | −9.89 | −9.82 | −9.45 | −9.13 |
| H−6 | −10.77 | −10.48 | −10.09 | −10.89 | −9.24 |
| H−7 | −10.86 | −10.53 | −10.67 | −11.09 | −10.19 |

**Table 5**
The vertical excitation wavelengths (nm), calculated oscillator strength (f) for transitions with $f > 10^{-3}$ and the classification of the transition (see text) including percentage contribution for $(\eta^6\text{-}C_6H_5Y)Cr(CO)_3$ (Y = H, or CHO)

| | nm | $f \times 10^4$ | Type (% contribution) |
|---|---|---|---|
| $(\eta^6\text{-}C_6H_6)Cr(CO)_3$ | 377.70 | 14 | MACT (58%) |
| | 377.67 | 14 | MACT (57%) |
| | 358.66 | 16 | MACT (52%) |
| | 358.64 | 16 | MACT (52%) |
| | 344.73 | 13 | MACT (74%) |
| | 344.71 | 13 | MACT (73%) |
| | 310.80 | 15 | MCCT (86%) |
| | 310.79 | 15 | MCCT (86%) |
| | 297.65 | 1893 | MACT (74%) |
| $(\eta^6\text{-}C_6H_5CHO)Cr(CO)_3$ | 427.79 | 537 | MACT (88%) |
| | 368.12 | 18 | MCCT (52%) |
| | 366.72 | 18 | MCCT (57%) |
| | 363.82 | 8 | MCCT (70%) |
| | 355.11 | 18 | MACT (65%) |
| | 309.82 | 170 | MCCT (68%) |
| | 307.11 | 431 | MCCT (59%) |
| | 302.42 | 1280 | MACT (41%) |

of the calculated transitions are presented in Table 5 and classified according to a coarse measure of the electron density drift. In the case of excited states where the electron density moves from the $Cr(CO)_3$ fragment to the arene ligand, the MACT (Metal to Arene Charge Transfer) label is applied. Transitions which result in a change of density from the $(\eta^6\text{-}C_6H_5Y)Cr$ fragment to the carbonyl ligands are labelled MCCT (Metal to Carbonyl Charge Transfer), these also contain significant Ligand Field (LF) character. In the case of $(\eta^6\text{-}C_6H_6)Cr(CO)_3$, the nature of the excited state changes from MACT to MCCT/LF as the excitation energy increases. A greater mix of excited state nature was obtained for $(\eta^6\text{-}C_6H_5CHO)Cr$-$(CO)_3$ however. Consequently these two complexes should exhibit different wavelength dependent behaviour.

The results of recent Time Resolved InfraRed (TRIR) experiments on $(\eta^6\text{-}arene)Cr(CO)_3$ systems, have been explained in terms of two excited states, whose surfaces undergo an avoided crossing at a Cr–CO distance greater than the equilibrium Cr–CO distance of the ground-state (Fig. 3) [20]. This results in a small but significant thermal barrier to loss of CO from the initially populated MACT excited state which is reflected in an unusually slow expulsion of CO (150 ps) following excitation at 400 nm at room temperature. Matrix isolation experiments would be expected to provide better information on the photochemistry resulting from
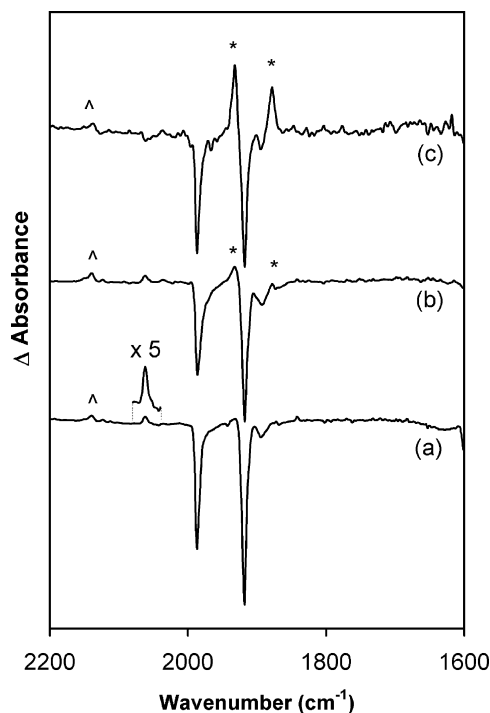
the population of either MACT or MCCT/LF excited states, as it is possible to systematically change the excitation wavelengths using steady-state sources.

### 2.4. Matrix isolation experiments

Low temperature matrix isolation studies were carried out on two complexes $(\eta^6\text{-}C_6H_6)Cr(CO)_3$ and $(\eta^6\text{-}C_6H_5CHO)Cr(CO)_3$ in a variety of matrix environments including $CH_4$ and 5% CO in $CH_4$. In general the methodology employed in these experiments involved initial photolysis using long wavelength excitation, moving to higher energy irradiation. The reactions were monitored by IR spectroscopy and in a few cases UV/Vis spectroscopy was used if the matrix quality permitted. In the case of matrix isolation spectra, data are presented in the form of IR difference absorbance in which the positive (upward) peaks represent the appearance of new species while negative (downward bleaches) represent photo-induced depletion. The irradiation source was a 200 W Xe/Hg lamp fitted with suitable interference filters which select specific Hg discharge lines.

### 2.5. Low temperature photochemistry of $(\eta^6\text{-}C_6H_6)Cr(CO)_3$ in a $CH_4$ matrix at 12 K

Despite the previously published work on the photochemistry of $(\eta^6\text{-}C_6H_6)Cr(CO)_3$ in low temperature matrixes [21], it was decided to revisit this system and to apply the same experimental methodology as applied to the substituted system described later. A $CH_4$ matrix containing $(\eta^6\text{-}C_6H_6)Cr(CO)_3$ exhibited $\nu_{CO}$ bands at 1987 and 1918 cm$^{-1}$. Photolysis of this matrix ($\lambda_{exc.}$ = 405 nm) resulted in depletion of the two bands. Weak features consistent with the formation of free CO were observed at 2138 cm$^{-1}$. In addition a weak feature was also observed at 2060 cm$^{-1}$ which we have tentatively assigned to a high energy mode of the triplet



**Fig. 3.** Proposed potential energy diagram for $(\eta^6\text{-}C_6H_6)Cr(CO)_3$ showing the avoided crossing of the MACT and MCCT/LF states at a Cr–CO distance greater than the ground state species. This results in a small thermal barrier to loss of CO such that $\Delta E$ is greater than $kT$ at 12 K, but small at room temperature.



**Fig. 4.** IR changes observed following photolysis of a $CH_4$ matrix containing $(\eta^6\text{-}C_6H_6)Cr(CO)_3$ at 12 K showing increasing formation of $(\eta^6\text{-}C_6H_6)Cr(CO)_2$ (*) with reducing excitation wavelength (a) 405 nm, (b) 365 nm and (c) 334 nm. The peak marked ^ corresponds to free CO. A weak peak at 2060 cm$^{-1}$ magnified in (a) has been tentatively assigned to the triplet $(\eta^6\text{-}C_6H_6)Cr(CO)_3$ species.

$(\eta^6\text{-}C_6H_6)Cr(CO)_3$ (Fig. 4). Reducing the excitation wavelength to 365 nm produced weak features at 1932 and 1878 cm$^{-1}$ consistent with the formation of $(\eta^6\text{-}C_6H_6)Cr(CO)_2$ (marked with * in Fig. 4). Further reduction of the excitation wavelength to 334 nm resulted in a significant increase in the formation of $(\eta^6\text{-}C_6H_6)Cr(CO)_2$ as observed by Rest et al. who used broad-band irradiation techniques but the weak feature at 2060 cm$^{-1}$ is depleted under these conditions [21].

### 2.6. The low temperature photochemistry of $(\eta^6\text{-}C_6H_5CHO)Cr(CO)_3$ in a CH$_4$ Matrix at 12 K

Visible photolysis ($\lambda_{exc.}$ = 405 nm) of a CH$_4$ matrix (12 K) containing $(\eta^6\text{-}C_6H_5CHO)Cr(CO)_3$ resulted in depletion of the bands of the parent compound and the production of two metal carbonyl bands at 1948 and 1896 cm$^{-1}$. In addition the carbonyl band of the aldehyde group in the parent was also depleted with the production of a new band at approximately 1680 cm$^{-1}$. As in the case of the benzene compound, these new features were assigned to the CO-loss product $(\eta^6\text{-}C_6H_5CHO)Cr(CO)_2$. Moving to higher energy photolysis ($\lambda_{exc.}$ = 365 nm) the bands of the CO-loss product were again observed but additional weak $\nu_{CO}$ bands at 1864, 1834, and 1816 cm$^{-1}$ were also produced (marked with square brackets in Fig. 5). The band at 1864 cm$^{-1}$ could be assigned to the Cr(CO)$_3$ fragment, the high energy band being obscured by the absorption of the parent tricarbonyl.[22] The origin of the remaining two bands is uncertain but they may indicate the formation of a "ring slip" species stabilised by interaction with the oxygen atom of the aldehyde group. Moving to yet higher energy photolysis ($\lambda_{exc.}$ = 334 nm) the CO-loss product was produced but now in the absence of the low-energy $\nu_{CO}$ bands at 1864, 1834, and 1816 cm$^{-1}$. Further monochromatic irradiation with $\lambda_{exc.}$ = 313 nm produced the bands of the CO-loss product together with the return of the bands at 1864, 1834, and 1816 cm$^{-1}$. In addition a broad feature is observed in the aldehyde carbonyl stretch region
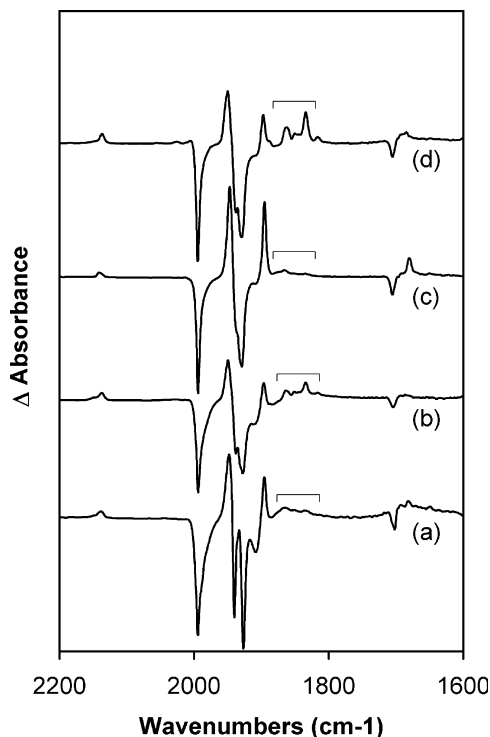


**Fig. 5.** The IR spectral changes observed following photolysis of a CH$_4$ matrix containing $(\eta^6\text{-}C_6H_5CHO)Cr(CO)_3$ at 12 K obtained following irradiation (a) at 405 nm, (b) 365 nm, (c) 334 nm and (d) 313 nm.

which indicates that the bands at 1864, 1834, and 1816 cm$^{-1}$ are associated with a complex in which the aldehyde group is involved in bonding to the metal (Reaction 3). This reaction is analogous to the proposed chelation of pendant sulphur-containing substituents following photochemical expulsion of CO from substituted $(\eta^5\text{-}C_5H_4Y)Mn(CO)_3$ systems [23].

Reaction 3
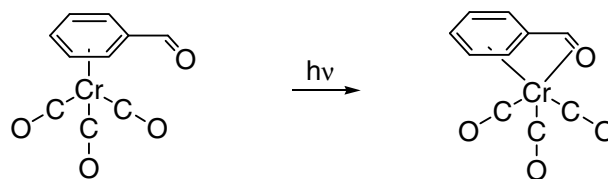


### 2.7. The low temperature photochemistry of $(\eta^6\text{-}C_6H_5CHO)Cr(CO)_3$ in a 2%CO–CH$_4$ matrix

Irradiation ($\lambda_{exc.}$ = 365 nm) of a 2% CO–CH$_4$ matrix (12 K) containing $(\eta^6\text{-}C_6H_5CHO)Cr(CO)_3$ produced the CO-loss product (1948 and 1895 cm$^{-1}$) along with weak features for the "ring slip" product at 1864, 1834 and 1816 cm$^{-1}$. However, these latter features are considerably weaker than those observed in the absence of CO. Two new features were observed at 2032 and 1960 cm$^{-1}$, the 1960 cm$^{-1}$ band appearing as a shoulder on the high-energy band of the CO-loss product. Thus it appears that the "ring slip" species reacts with CO. We have tentatively assigned the band 1960 cm$^{-1}$ to a complex containing a metal pentacarbonyl fragment $((\eta^x\text{-}C_6H_5CHO)Cr(CO)_5)$ the remaining strong band being obscured by the parent bands. The high energy $A_1$ mode is too weak to be observed in these experiments. The band at 2032 cm$^{-1}$ may correspond to the high energy mode of a tetracarbonyl fragment, again the remaining bands of this fragment being obscured by parent absorptions.

Reducing the wavelength to 313 nm produced the CO-loss product and the metal carbonyl fragment absorbing at 1864, 1834, and 1816 cm$^{-1}$. Subsequent photolysis of this matrix with broadband light ($\lambda_{exc.}$ > 320 nm) produced a significant yield of Cr(CO)$_6$ at the expense of the bands at 1864, 1834, and 1816 cm$^{-1}$. This suggests that the "ring slip" species is a precursor to Cr(CO)$_6$, and that the ultimate fission of the chromium–arene bond requires the absorption of more than one photon under these conditions.

## 3. Discussion

The dominant photochemical process for $(\eta^6\text{-}C_6H_5Y)Cr(CO)_3$ (Y = NH$_2$, OCH$_3$, H, COH, CO$_2$CH$_3$) in room temperature alkane solution is loss of one CO ligand. This process has a high quantum yield (0.72 for Y = H; $\lambda_{exc.}$ = 313 nm) [11]. The quantum yield of arene loss is low, (0.01 for Y = H), and is essentially zero for Y = H when the photolysis is conducted in the presence of added CO [24]. This observation led previous workers to conclude that the arene loss process occurred subsequent to an initial CO loss. However, our investigations indicate that the CO loss and arene loss are the result of two distinct photo-physical processes.

The quantum yields of the arene-loss processes were measured by monitoring spectroscopic changes which occurred following irradiation of CO-saturated solutions in either hydrocarbon or halocarbon solutions. In all cases the products of these reactions were Cr(CO)$_6$ and the uncoordinated arene as verified by both IR and $^1$H NMR spectroscopy. The reduction in the absorbance at their $\lambda_{max.}$ was used to measure the photoinduced depletion of $(\eta^6\text{-}$

$C_6H_5Y)Cr(CO)_3$ (Y = H, $NH_2$, $OCH_3$, CHO, $CO_2CH_3$) per unit photon flux, as neither $Cr(CO)_6$ or the uncoordinated arene ligand absorb significantly at these wavelengths.

The results outlined in Table 2 show that the quantum yield of arene loss is strongly dependent on the nature of the solvent, being greater in halocarbon solvent than in hydrocarbon solvent. These results are consistent with the previously published results of Bamford [25], who measured the quantum yield of arene loss from $(\eta^6\text{-}C_6H_6)Cr(CO)_3$ to be 0.41 ($\lambda_{exc.}$ = 365 nm) in $CCl_4$. Solvent effect on the quantum yield of CO-loss from $Cr(CO)_6$, have been observed. For instance a quantum yield of 0.3 was obtained for perfluorodecalin compared to 0.67 in cyclohexane [26]. However, the lower quantum yield in perfluoro-solvents was explained by a more efficient recombination of the $Cr(CO)_5$ fragment with the ejected CO in the perfluoro-solvent cage. Such a process could not explain our observations.

Flash photolysis experiments indicate that both processes occur on the sub-nanosecond timescale. However, in contrast to the photoinduced CO-loss from $Cr(CO)_6$ which occurs on the sub-picosecond timescale [27,28] and before significant vibrational relaxation can occur, CO-loss from $(\eta^6\text{-}C_6H_6)Cr(CO)_3$ is slow and occurs on the 100–200 ps timescale [20]. The rate of vibrational relaxation may affect the direction of the photochemical process by facilitating reaction from higher vibrational levels on the excited state surface. This may be the reason why the quantum yield of arene loss is greater in halocarbon solvent.

The TDDFT calculations provide information on the prevailing nature of the optically assessable excited states. In the case of Y = H the lower energy transitions are predominantly MACT in character, and the MCCT/LF state is accessible only upon moving to higher energy irradiations. The TDDFT results for Y = CHO indicate that the nature of the excited state is less polarised between MACT and MCCT/LF states. This means that both CO-loss and the ring slip process will occur at all excitation wavelengths as presented in Fig. 5.

Another interesting feature of the photochemistry of $(\eta^6\text{-}$benzene$)Cr(CO)_3$ is that at room temperature photolysis at 400 nm results in efficient formation of $(\eta^6\text{-}$benzene$)Cr(CO)_2(S)$ in alkane solvents (S). However, similar photolyses ($\lambda_{exc.}$ = 405 nm) in low temperature matrixes (Fig. 4) failed to produce a significant yield of the CO-loss species. We have explained this observation by proposing the initial population of a Metal to Arene Charge Transfer (MACT) excited state. This excited state is a bound state, and ultimately relaxes to the ground state by non-radiative processes. However this MACT state undergoes an avoided crossing with the higher energy Metal to Carbonyl Charge Transfer/Ligand Field state (MCCT/LF) at a Cr–CO distance greater than the equilibrium Cr–CO distance in the ground state. This produces a small but significant thermal barrier to the loss of one CO ligand (Fig. 3). Consequently, following irradiation at 400 nm an additional thermal barrier must be overcome on the reaction coordinate to CO loss. If higher energy photons are used these can directly populate the MCCT state and the conical intersection at the avoided crossing provides access to the region of the potential energy hyper-surface which is unbound with respect to the Cr–CO interaction (Fig. 3).

It is interesting to compare the behaviour of $(\eta^6\text{-}C_6H_6)Cr(CO)_3$ with that of $(\eta^6\text{-}C_6H_5CHO)Cr(CO)_3$. Low energy photolysis of $(\eta^6\text{-}C_6H_5CHO)Cr(CO)_3$ in a $CH_4$ matrix ($\lambda_{exc.}$ = 405 nm) produced peaks at 1948 and 1896 $cm^{-1}$ consistent with the CO-loss species $(\eta^6\text{-}C_6H_5CHO)Cr(CO)_2$ while, as mentioned above, similar photolysis of $(\eta^6\text{-}C_6H_6)Cr(CO)_3$ failed to produce the CO-loss species. Thus it would appear that the presence of the aldehyde substituent on the arene ligand increases the efficiency at which CO is lost under low-energy photolysis, an observation which is consistent with the TDDFT calculations. In addition peaks consistent with a reduced hapticity of the arene ligand were observed for $(\eta^6\text{-}C_6H_5CHO)$-

$Cr(CO)_3$ but not for $(\eta^6\text{-}C_6H_6)Cr(CO)_3$. This is because the aldehyde group on the arene ligand can act as a "trap" for ring-slip intermediates. Experiments conducted in the presence of CO confirmed that this intermediate reacts with CO to form higher order metal carbonyl complexes and ultimately $Cr(CO)_6$.

## 4. Concluding comments

The photochemical experiments conducted with monochromatic irradiation have conclusively shown that CO-loss and arene-loss from $(\eta^6\text{-}$arene$)Cr(CO)_3$ complexes result from discrete photophysical processes. The quantum yields of these processes depend on the nature of the solvent which suggests that vibronic coupling in the excited states is important in determining the nature of the observed photochemistry. Further work in ongoing on the photochemistry of $(\eta\text{-}$heteroaromatic$)M(CO)_3$ systems (M = Cr, Mo, or W) with a view to understanding the photophysical process preceding photoinduced arene loss.

## 5. Experimental

Quantum yield determinations were made using standard ferrioxalate actinometry using the 355 nm Nd-YAG line as the light source [29]. Sample concentrations were adjusted to produce an absorbance of 1 at 355 nm, and the destruction of the parent $(\eta^6\text{-}C_6H_5Y)Cr(CO)_3$ species was monitored by the change in the absorbance at 355 nm. The photon flux per laser pulse was measured using the ferrioxalate actinometer and the pulse stability was monitored using a power meter coupled to a storage oscilloscope. Measurements were repeated until a consistent value was obtained, representing a variance of ±5% for quantum yields above 0.1 and ±20% for quantum yields below 0.1.

## 6. Theoretical calculations

All calculations were carried out using the Gaussian 98 or the the GAUSSIAN03 program revision C.02 running on a dual Xeon processor workstation (3.6 GHz) under Windows XP [12,13]. The model chemistry employed in all calculations used the Becke three parameter hybrid functionals [30], using the correlation function of Lee, Yang and Parr which includes both local and non-local terms [31]. The LANL2DZ basis set was used for all calculations which employs the Dunning/Huzinaga valence double-zeta functions for the first row elements [32], and the Los Alamos effective core potentials plus double zeta functions on elements from Na to Bi [33–35]. Time-Dependent DFT calculations used the geometry obtained from an optimisation at the B3LYP/LANL2DZ model chemistry. The TDDFT calculations examined only the twenty lowest energy singlet states. The GAUSSSUM package [15] was used to obtain the contribution to specific Kohn Sham orbitals made by specific molecule fragments namely the three CO ligands, the metal atom and finally the benzene ligand (see Supporting Information for details).

## 7. Apparatus

Spectra were recorded on the following instruments: IR, Perkin-Elmer 2000 FT-IR (2 $cm^{-1}$ resolution), UV/Vis. Hewlett-Packard 8452A; NMR, Brüker AC 400.

The laser flash photolysis apparatus has been described previously [36]. For this work, the 355 nm line of a pulsed Nd:YAG laser was used (energy approximately 35 mJ per pulse; system response 10 ns). Solutions for analysis were placed in a fluorescence cuvette ($d$ = 1 cm) attached to a degassing bulb and were degassed by three cycles of freeze-pump-thaw to $10^{-2}$ Torr, followed by liquid pump-

ing to remove traces of water (this typically removed half the original volume of solvent). The absorbance of the solution at the excitation wavelength was adjusted to lie in the range 0.5–1.0. The UV/Vis. spectrum of the sample solution was monitored throughout the experiments to monitor changes in absorbance.

The matrix isolation apparatus consists of a closed cycle helium refrigerator, sample window, shroud, deposition tube, gas mixing chamber, gas inlet, backing pump, diffusion pump and temperature control unit. Matrices were deposited onto a $CaF_2$ window cooled to 20 K, with matching outer windows on the vacuum shroud. A thermocouple embedded into a cavity beside the window and connected to the temperature control unit maintains the temperature. The window is cooled, by a closed cycle helium refrigerator (APD Cryogenics Inc.), mounted via a double O-ring seal in a stainless steel vacuum shroud. The system pumps to $8 \times 10^{-4}$ Torr prior to cooling and achieves $10^{-7}$ Torr upon cooling to 20 K. Host gases (Cryo Service) are deposited onto a window via a needle valve. For mixed gas matrices, the gasses are mixed in the correct ratio in the stainless steel mixing chamber prior to deposition. A ratio of sample molecule to host matrix in the region 1:2000 is desirable. Typically a rate of gas deposition of 0.6 Torr per min. achieves sufficient dilution on the matrix window. Both the sample and gas are deposited simultaneously. Deposition was stopped when the $v_{CO}$ absorbance was approximately 1 A.U. Once the required absorbance was achieved the sample was photolysed and monitored on a Spectrum One FTIR spectrophotometer fitted with a KBr beam splitter. Spectra were recorded at 1 cm$^{-1}$ resolution. UV/Vis. spectra were recorded on a Perkin-Elmer Lambda EZ201 spectrophotometer. Matrixes were photolysed through a $CaF_2$ window with a 300 W-Xe arc or 200 W Hg–Ar lamp in combination with a water filter. Photolysis wavelengths were selected with cut-off or interference filters.

## 8. Materials

The following solvents were of spectroscopic grade and used without purification; cyclohexane, heptane and 1,1,2 triflourotrichloroethane (Aldrich chemicals).

Argon and carbon monoxide were supplied by Air Products and BOC. Carbon monoxide and methane for matrix isolation were obtained from Cryogas, $(\eta^6\text{-}C_6H_5CO_2CH_3)Cr(CO)_3$ and $(\eta^6\text{-}C_6H_6)Cr(CO)_3$ (Aldrich chemicals) were used without further purification.

### 8.1. The synthesis of $(\eta^6\text{-}C_6H_5NH_2)Cr(CO)_3$

$Cr(CO)_6$ (0.4 g, 1.8 mmol), $C_6H_5NH_2$ (2.4 g, 24.73 mmol) dibutyl ether (12 ml) and freshly distilled THF (1 cm$^3$) were heated under reflux under an nitrogen atmosphere for 24 h yielding a yellow–orange solution. When cool the solution was filtered through Celite and the solvent removed under reduced pressure, at room temperature leaving a dark yellow oil. Upon addition of cold pentane, a fine yellow powder formed. This powder was recrystallised from a toluene-pentane mixture (70% yield based on $Cr(CO)_6$). $v_{co}$ bands (cyclohexane):1967, 1893 and 1888 cm$^{-1}$. NMR (CDCl$_3$): 5.56 (dd, 2H) and 4.79 (m, 3H) ppm.

### 8.2. The synthesis of $(\eta^6\text{-}C_6H_5OCH_3)Cr(CO)_3$

$Cr(CO)_6$ (0.4 g, 1.8 mmol), $C_6H_5OCH_3$ (2.8 g, 25.9 mmol) dibutyl ether (12 ml) and freshly distilled THF (1 ml) were heated to reflux temperature under a nitrogen atmosphere for 24 h in the dark. The resulting yellow-orange solution was cooled and filtered through celite. The solvent was then removed under reduced pressure leaving a dark yellow oil. A yellow powder formed upon addition of pentane. This powder was recrystallised from a toluene-pentane mixture yielding 360 mg (% yield 82% based on $Cr(CO)_6$). $v_{co}$ bands (cyclohexane): 1978, 1908 cm$^{-1}$. NMR (CDCl$_3$): 5.56 (d, 2H), 5.10 (dd, 3H), 4.87 (s, 1H) and 3.81 (s, 3H) ppm.

### 8.3. The synthesis of benzaldehyde diethyl acetal

Benzaldehyde diethyl acetal was synthesised by a published procedure [37], which involved treatming a mixture of benzaldehyde (11 g, 0.104 mole) and ethyl orthoformate (15.1 g, 0.102 mole) with two drops of concentrated sulphuric acid followed by stirring for 24 h. Sodium carbonate 0.2 g was then added to neutralise the excess acid. The solution was filtered and distilled under reduced pressure to afford 11.75 g (64%) of benzaldehyde diethyl acetal, B.P. 96–99 °C/11–15 mm Hg. $^1$H NMR 7.33, 7.163, 5.37, 3.46 ppm.

### 8.4. The synthesis of $(\eta^6\text{-}C_6H_5CH(OC_2H_5)_2)Cr(CO)_3$

A modification of a literature procedure was used for this synthesis [38]. A solution containing chromiumhexacarbonyl (0.4 g,1.8 mmol) and benzaldehyde diethylacetal (2.4 g, 24.73 mmol) in dioxane (12 ml) was heated at reflux temperature under a nitrogen atmosphere for 10 h. The yellow solution was cooled and filtered through celite on a sintered-glass filter. The solvent was removed under reduced pressure at room temperature and the yellow solid washed with cold pentane. The crude product was used for the preparation of $(\eta^6\text{-}C_6H_5CHO)Cr(CO)_3$ without further purification. The compound was characterised by IR spectroscopy $v_{CO}$ bands (pentane): 1981, 1914 cm$^{-1}$.

### 8.5. The synthesis of $(\eta^6\text{-}C_6H_5CHO)Cr(CO)_3$

A solution containing 0.27 g of $(\eta^6\text{-}C_6H_5CH(OC_2H_5)_2)Cr(CO)_3$ and 30 ml of 0.5 M HCl was stirred at room temperature for four hours. The product $(\eta^6\text{-}C_6H_5CHO)Cr(CO)_3$ was extracted into diethylether and recovered by removal of the solvent under reduced pressure. The resulting solid was recrystallised from pentane to give orange crystals of $(\eta^6\text{-}C_6H_5CHO)Cr(CO)_3$. $v_{CO}$ bands(cyclohexane): 1995, 1940, and 1931 cm$^{-1}$ and 1707 cm$^{-1}$, $^1$H NMR 9.392 (1H), 5.887, 5.872 (2H), 5.627 (1H), 5.242, 5.226, 5.21 (2H) ppm.

## Acknowledgements

## Appendix A. Supplementary data

Supplementary data associated with this article can be found, in the online version, at doi:10.1016/j.jorganchem.2008.06.003.

## References

[1] G.L. Geoffroy, M.S. Wrighton, Organometallic Photochemistry, Academic Press, New York, 1979.
[2] W. Strohmeier, K. Gerlach, Z. Naturforsch. B 15 (1960) 622.
[3] N.A. Beach, H.B. Gray, J. Am. Chem. Soc. 90 (1968) 5713.
[4] P. Hummel, J. Oxgaard, W.A. Goddard, H.B. Gray, Inorg. Chem. 44 (2005) 2454.
[5] K. Pierloot, J. Verhulst, P. Verbeke, L.G. Vanquickenborne, Inorg. Chem. 28 (1989) 3059.
[6] C. Pollak, A. Rosa, E.J. Baerends, J. Am. Chem. Soc. 119 (1997) 7324.
[7] S. Villaume, A. Strich, C. Daniel, S.A. Perera, R.J. Bartlett, Phys. Chem. Chem. Phys. 9 (2007) 6115.
[8] S.M. Arrivo, T.P. Dougherty, W.T. Grubbs, E.J. Heilweil, Chem. Phys. Lett. 235 (1995) 247.
[9] T.H. Chang, J.I. Zink, Inorg. Chem. 24 (1985) 4016.

[10] C.J. Breheny, S.M. Draper, F.W. Grevels, W.E. Klotzbucher, C. Long, M.T. Pryce, G. Russell, Organometallics 15 (1996) 3679.
[11] M.S. Wrighton, J.L. Haverty, Z. Naturforsch. B 30 (1975) 254.
[12] M.J. Frisch, G.W. Trucks, H.B. Schlegel, G.E. Scuseria, M.A. Robb, J.R. Cheeseman, V.G. Zakrzewski, J.A. Montgomery, Jr.;, R.E. Stratmann, J.C. Burant, S. Dapprich, J.M. Millan, A.D. Daniels, K.N. Kudin, M.C. Strain, O. Farkas, J. Tomasi, V. Barone, M. Cossi, R. Cammi, B. Mennucci, C. Pomelli, C. Adamo, K. Morokumma, D.K. Malick, A.D. Rabuck, K. Raghavachari, J.B. Foresman, J. Cioslowski, J.V. Ortiz, A.G. Baboul, B.B. Stefanov, G. Liu, A. Liashenko, P. Piskorz, I. Komaromi, Y. Gomperts, A. Nanayakkaara, C. Gonzalez, M. Challacombe, P.M.W. Gill, B. Johnson, W. Chen, M.W. Wong, J.L. Andres, C. Gonzalez, M. Head-Gordon, E.S. Replogle, J.A. Pople, GAUSSIAN98, revision A. 7, Gaussian Inc., Pittsburgh, PA, USA, 1998.
[13] M.J. Frisch, G.W. Trucks, H.B. Schlegel, G.E. Scuseria, M.A. Robb, J.R. Cheeseman, J.J.A. Montgomery, T. Vreven, K.N. Kudin, J.C. Burant, J.M. Millam, S.S. Iyengar, J. Tomasi, V. Barone, B. Mennucci, M. Cossi, G. Scalmani, N. Rega, G.A. Petersson, H. Nakatsuji, M. Hada, M. Ehara, K. Toyota, R. Fukuda, J. Hasegawa, M. Ishida, T. Nakajima, Y. Honda, O. Kitao, H. Nakai, M. Klene, X. Li, J.E. Knox, H.P. Hratchian, J.B. Cross, C. Adamo, J. Jaramillo, R. Gomperts, R.E. Stratmann, O. Yazyev, A.J. Austin, R. Cammi, C.J. Pomelli, W. Ochterski, P.Y. Ayala, K. Morokuma, G.A. Voth, P. Salvador, J.J. Dannenberg, V.G. Zakrzewski, S. Dapprich, A.D. Daniels, M.C. Strain, O. Farkas, D.K. Malick, A.D. Rabuck, K. Raghavachari, J.B. Foresman, J.V. Ortiz, Q. Cui, A.G. Baboul, S. Clifford, J. Cioslowski, B.B. Stefanov, G. Liu, A. Liashenko, P. Piskorz, I. Komaromi, R.L. Martin, D.J. Fox, T. Keith, M.A. Al-Laham, C.Y. Peng, A. Nanayakkara, M. Challacombe, P.M.W. Gill, B. Johnson, W. Chen, M.W. Wong, C. Gonzalez, J.A. Pople, GAUSSIAN03, Gaussian Inc., Wallingford CT, 2004.
[14] GAUSSVIEW 3.0, Gaussian Inc., Pittsburgh, PA, USA, 2003.
[15] N.M. O'Boyle, GAUSSSUM, 2006.
[16] A. Bérces, T. Ziegler, J. Phys. Chem. 99 (1995) 11417.
[17] K.B. Wiberg, R.E. Statmann, M.J. Frish, Chem. Phys. Lett. 297 (1998) 60.
[18] R. Bauernschmitt, R. Ahlrichs, Chem. Phys. Lett. 256 (1996) 454.
[19] R.E. Stratman, G.E. Scuseria, M.J. Frisch, J. Chem. Phys. 109 (1998) 8218.
[20] (a) M.A.H. Alamiry, N.M. Boyle, M.W. George, C. Long, M.T. Pryce, K.L. Ronayne, M. Towrie (in preparation).;

(b) M.T. Pryce, N.M. Boyle, A. Coleman, C. Long, W.R. Browne, B.L. Feringa, K.L. Ronayne, M. Towrie, Probing early picosecond dynamics in transition metal complexes using PIRATE, Central Laser Facility Annual Report, Rutherford Appleton Laboratory, Oxford, 2006/2007, pp. 141.
[21] A.J. Rest, J.R. Sodeau, D.J. Taylor, J. Chem. Soc., Dalton Trans. (1978) 651.
[22] R.N. Perutz, J.J. Turner, J. Am. Chem. Soc. 97 (1975) 4800.
[23] T.T. To, E.J. Heilweil, T.J. Burkey, J. Phys. Chem. A 110 (2006) 10669.
[24] A. Gilbert, J.M. Kelly, M. Budzwatt, E. Koerner von Gustorf, Z. Naturforsch. 31b (1976) 1091.
[25] C.H. Bamford, K.G. Al-Lamee, C.J. Konstantinov, J. Chem. Soc. (1977) 1406.
[26] S.K. Nayak, T.J. Burkey, Organometallics 10 (1991) 3745.
[27] M. Gutmann, M.S. Dickebohm, J.M. Janello, J. Phys. Chem. A 103 (1999) 2580.
[28] M. Gutmann, J.M. Janello, M.S. Dickebohm, M. Grossekathofer, J. Lindener-Roenneke, J. Phys. Chem. A 102 (1998) 4138.
[29] P. Brennan, The Photochemical Properties of Arene Metal Carbonyl Complexes of Group 6 and 7 Elements, Dublin City University, Dublin, 2003.
[30] A.D. Becke, J. Chem. Phys. 98 (1993) 5648.
[31] C.T. Lee, W.T. Yang, R.G. Parr, Phys. Rev. B 37 (1988) 785.
[32] T.H. Dunning Jr, P.J. Hay, in: H.F. Schaefer (Ed.), Modern Theoretical Chemistry, Plenum, New York, 1976, pp. 1–28.
[33] P.J. Hay, W.R. Wadt, J. Chem. Phys. 82 (1985) 270.
[34] P.J. Hay, W.R. Wadt, J. Chem. Phys. 82 (1985) 299.
[35] W.R. Wadt, P.J. Hay, J. Chem. Phys. 82 (1985) 284.
[36] B.S. Creaven, M.W. George, A.G. Ginzburg, C. Hughes, J.M. Kelly, C. Long, I.M. McGrath, M.T. Pryce, Organometallics 12 (1993) 3127.
[37] M.D. Rausch, G.A. Moser, E.J. Zaiko, A.L. Lipman, J. Organomet. Chem. 23 (1970) 185.
[38] G. Drehfahl, H.H. Horhold, K. Kuhne, Chem. Berl. 98 (1965) 1826.
[39] M.J. Calhorda, C.F. Frazao, J.A. Martinho-Simões, J. Organomet. Chem. 262 (1984) 305.
[40] A.D. Hunter, L. Shilliday, W.S. Furey, M.J. Zaworotko, Organometallics 11 (1992) 1550.
[41] J.Y. Saillard, D. Grandjean, Acta Crystallogr. Sect. B 32 (1976) 2285.